Document Title:	**MERIS aerosol remote sensing over land**
Version:	5
Author(s):	R. Santer[1] and D. Ramon[2]
Affiliation(s):	(1) ULCO, Université du Littoral Côte d'Opale, Wimereux - France.
	(2) HYGEOS,165 Avenue de Bretagne 59000 Lille, France
Modification History:	MERIS 3rd reprocessing
Distribution:	Public

Acronyms

ARVI	Atmospheric Resistant Vegetation Index
AOT	Aerosol Optical Thickness
ATBD	Algorithm Theoretical Basic Document
BRDF	Bidirectional Reflectance Distribution Function
CCI	Climate Change Initiative
DDV	Dense Dark Vegetation
ESA	European Space Agency
LARS	Land Aerosol Remote Sensing
LUT	Look Up Table
MERIS	MEdium Resolution Imaging Spectrometer
MEGS	MERIS Ground Segment
MODIS	Moderate Resolution Imaging Spectroradiometer
POLDER	POLarization and Directionaly of Earth Reflectance
SAM	Standard Aerosol Model
TOA	Top Of Atmosphere

1) Introduction

The objective of this technical note is to update the ATBD-15: *Atmospheric products over land for MERIS level 2.*(http://envisat.esa.int/instruments/meris/atbd/atbd_2_15.pdf). The Rayleigh correction is unchanged to deliver the L2 so-called surface reflectance. A new surface pressure algorithm was developed by Fischer J. and collaborators. We are here concerned by the modifications of the aerosol remote sensing over land. The reference document produced by HYGEOS in the frame of a CCI is annexed to this report. The fundamental principle is first to use land pixels covered by the vegetation in the blue and red spectral bands for which the vegetation is dark and second to characterize the aerosols by fitting at the best MERIS TOA reflectance in those spectral bands by pre-computed predicted values associated to an aerosol model.

The fundamental bases of this algorithm are:
(i) The use of the TOA reflectance measured over clear sky pixels over land after correction of the gaseous absorption.
(ii) The identification of the so-called LARS pixels using the L2 reflectance (Rayleigh corrected) and the ARVI.
(iii) An auxiliary data base of the albedo of those LARS pixels in B1, B2 and B7 (412 nm, 442 nm and 670 nm). A coarse albedo map was initially provided by POLDER.
(iv) A BRDF correction of the albedo to get the reflectance of the LARS pixels in the MERIS geometrical conditions.
(v) A set of 26 standard aerosol models (SAM): Power law particle size distribution with a slope associated to the Angstrom coefficient α, non absorbing spherical particles with a refractive index of 1.44.
(vi) LUT of the aerosol scattering functions for these 26 SAM in B1, B2 and B7.
(vii) LUT of corrective coefficients to account for the bi-directionality of the coupling terms between aerosol and molecular scattering, atmospheric scattering and surface reflection.
(viii) Retrieval of the aerosol product (AOT at 442 nm and α) based on the best retrieval of the MERIS TOA reflectance in B1, B2 and B7.

Basically, points (i), (ii), (iv), (v), (vi), (vii) and (viii) were unchanged since the beginning of the mission.

The second reprocessing (MEGS7.5) aimed to extend the concept of DDV to "less dark" pixels in order to improve the spatial coverage of the aerosol product. The major effort was brought on point (iii) through the generation of a data base of the LARS reflectance. The LARS reflectance is assumed to be linear with the ARVI in a certain domain and the MODIS global albedo product was used to generate the auxiliary data. The knowledge of the LARS reflectance at 670 nm is quite inaccurate resulting in a poor determination of α. It was decided to decouple the retrieval of the AOT in B2 from the retrieval of α. In B2, the AOT corresponds to a retrieval with $\alpha = -1$.

2) MEGS 8.0

A MERIS albedo map product (http://www.brockmann-consult.de/albedomap/) was made available and of course offers a better spectral matching than MODIS. Therefore, it was decided to generate a new set of LARS reflectance.

The second point brings on the simplification of the algorithm: only B2 and B7 are used to retrieve the AOT_440 and α.

3) Recommendations

Clearly the aerosol retrieval over land using MERIS is not a ESA priority of the mission and several recommendations made since many years needs to be considered first on the existing L2:

(i) The two band algorithm follows the same logic that the former three band algorithm and should be redefined and simplified for time efficiency.

(ii) The BRDF correction is conducted with a BRDF model defined with POLDER and corresponding to DDV. This BRDF model should be defined for "less dark" vegetation and defined by classes of ARVI.

(iii) The 26 SAM should be replaced by more realistic aerosol models or inherent aerosol optical properties.

(iv) The selected aerosol model to derive the AOT at 442 nm should be redefined in accordance with the aerosol climatology.

(v) The two band algorithm should be deeply evaluated with B1 and B2. The trade off with B2-B7 is between the spectral interval (larger between B2 and B7) and the darkness of the vegetation (deeper in B2 compared to B7)

(vi) The smile effect should be accounted for the Rayleigh computation.

But clearly at the end we will have an inconsistent algorithm with a determination of α which does not impact on the determination of the AOT (derived with a standard value of α). There is a need to introduce additional information, which can be based on a better spatial homogeneity of α than of the AOT. That means that we do not have a pixel by pixel algorithm.

One possible algorithm is:

The current algorithm is applied except than we retain the 26 values of the AOT derived for the 26 SAM in B2. This algorithm outputs, for each LARS pixel, a vector AOT in B2 and α.

A post processor to L2 applies to each land pixel with:

(i) Open a window N*N RR pixels; N=9 is the nominal value.

(ii) After filtering, derived the most likely value of α and associated AOT.

(iii) The vegetation is darker in B2 compared to B7. Therefore, we can select a lower value of the ARVI threshold to derive the AOT for new LARS pixels.

At the end of this aerosol retrieval, we will have an aerosol model for each land pixel. It renders possible to include in the atmospheric correction the aerosols.

EXECUTIVE SUMMARY

The document describes the basis of the algorithm for retrieving aerosol over land with the MERIS instrument that is implemented in the MERIS level 2 ground segment. The MERIS standard aerosol retrieval over land algorithm was designed to work over Dense Dark Vegetation (DDV) targets. A set of DDV Bidirectional Reflectance Function (BRF) models was assembled for 11 different biomes on Earth. DDV detection is based on a threshold on the Atmospherically Resistant Vegetation Index (ARVI) computed from Rayleigh corrected reflectances at 443, 665 and 865 nm. As DDV spatial cover is low, the aerosol inversion was extended to brighter surfaces called Land Aerosol Remote Sensing (LARS) targets. LARS spectral albedo can be predicted as it is linearly related to ARVI. Slopes and offsets of these linear regressions are stored in Look Up Tables for 1°x1° boxes and on a monthly basis. The aerosol retrieval consists in the inversion of the Aerosol Optical Thickness at 443 and 665 nm that allow to reproduce the measured Top Of Atmosphere (TOA) reflectances at 443 and 665 nm using pre-calculated aerosol scattering functions for aerosol models described by a Junge Power-Law (JPL) size distribution and a constant refractive index of 1.45-0.0i. The outputs of the algorithm are the AOT at 443 nm and the aerosol Ångström exponent derived between 443 and 665 nm.

Cloud contamination is the biggest issue of the product that is delivered at the same spatial resolution as the level 1B data (i.e 1.2 km). The product, with a good spatial coverage now, has been validated only for the AOT at 443 nm. The Ångström exponent is not validated since the retrieved AOT at 665 nm is noisy. It is mandatory to move toward spatial resolution of 10 km for the aerosol product in order to reduce cloud contamination and enhance the Signal to Noise Ratio (SNR) for the Ångström exponent retrieval. Finally there is a need for improving the LARS BRDF model.

LIST OF TABLES

N/A

LIST OF FIGURES

TABLE OF CONTENTS

INTRODUCTION

This document describes the theoretical basis for the aerosol retrieval algorithm developed for MERIS by Université du Littoral. This algorithm is referred to as ESA standard aerosol product over land. The algorithm forms the basis for further development and in improvement in the Aerosol-cci project.

Scope

The MERIS ESA standard aerosol product over land has been extensively described in a series of peer-reviewed papers and reports. This ATBD aims to provide an overview of the algorithm with detailed references to the above-mentioned papers and reports as well as ATBD's already published on the ESA MERIS web page, with summaries of the issues that are important for the aerosol-cci work. It will not be a comprehensive compilation of all existing literature.

References

Applicable Documents

4) Statement of Work "ESA Climate Change Initiative Stage 1, Scientific user Consultation and Detailed Specification", ref EOP-SEP/SOW/0031-09/SP. Issue 1.4, revision 1, dated 9 November, 2009, together with its Annex C "Aerosols" (altogether the SoW).

5) The Prime Contractor's Baseline proposal, ref. 3003432, Revision 1.0, dated 16 June 2010, and the minutes of the July 26, 2010 kick-off meeting.

6) Aerosol-cci project management plan (PMP), version 1.3.

7) MERIS ENVISAT Handbook available from http://earth.esa.int/pub/ESA_DOC/ENVISAT/MERIS/meris.ProductHandbook.2_1.pdf

8) MERIS level 2 pixel classification ATBD are available from http://envisat.esa.int/instruments/meris/atbd/atbd_2_17.pdf

9) MERIS level 2 atmospheric products over land ATBD http://envisat.esa.int/instruments/meris/atbd/atbd_2_15.pdf

10) MERIS level 2 aerosol retrieval over land accounting for directional effects ATBD http://envisat.esa.int/instruments/meris/atbd/atbd_2_19.pdf

11) Specification of the scientific contents of the MERIS level-1b & 2 auxiliary data products, ParBleu report (PO-RS-PAR-GS-0002-3B): 'ENVISAT-1 Ground segment for MERIS', F. Zagolski , St Jean-sur-Richelieu (Qc), Canada, February 2011: 537 p.

12) MERIS level 2 Detailed Processing Model (PO-TN-MEL-GS-0002)

13) MERIS Input / Output Data Definition IODD (PO-TN-MEL-GS-0003)

14) Envisat-1 Product Specifications (PO-RS-MDA-GS-2009) Volume 11 MERIS Products

15) Technical note: MERIS IPF releases, available from

http://earth.eo.esa.int/pcs/envisat/meris/documentation/MERIS_IPF_evolution.pdf

16) MERIS wavelengths and irradiances model (2004), available from

http://earth.eo.esa.int/pub/ESA_DOC/MERIS_Wavelengths_and_Irradiances_Model2004.xls

Reference Documents

[RD1] Santer, R., Carrere, V., Dubuisson, P. and Roger, J. C. (1999) Atmospheric correction over land for MERIS. *International Journal of Remote Sensing*, **20**, pp. 1819-1840.

[RD2] Santer R., Ramon D., Vidot J., Dilligeard E., (2007), A Surface Reflectance Model for Aerosol Remote Sensing over Land. *International Journal of Remote Sensing*. Vol **28**.

[RD3] Ramon D. and R. Santer, "Operational remote sensing of aerosols over land to account for directional effects", *Applied Optics-LP*, **40**, 3060-3075, (2001)

[RD4] Ramon D. and R. Santer, (2008), "Validation of the aerosol product over land", *Second MERIS-AATSR Workshop*, 22-26 September 2008, ESA-ESRIN, Frascati, Italy, 2008, presentation available at:

http://earth.esa.int/workshops/meris_aatsr2008/participants/800/pres_800_Ramon.pdf

[RD5] BORDE R., RAMON D., SCHMECHTIG C., SANTER R.. (2003) Extension of the DDV concept to retrieve aerosol properties over land from the Modular Optoelectronic Scanner sensor. *International Journal of Remote Sensing*, vol **24**, No 7, 1439-1467.

[RD6] SANTER R., ZAGOLSKI F., RAMON D., FISCHER J., DUBUISSON P., (2005) Uncertainties in Radiative Transfer Computations, Consequences on the MERIS products over land, *International Journal of Remote Sensing*. Vol. **26**, No. 20, 20 October 2005, 4597–4626

[RD7] SCHMECHTIG C., CARRERE V., DUBUISSON P., ROGER J.-C. and SANTER R.(2003). Sensitivity analysis for the aerosol retrieval over land for MERIS . *International Journal of Remote Sensing*, Vol **24**, No14, 2921-2944.

[RD8] Ramon, D., R. Santer, E. Dilligeard and D. Jolivet, (2003) MERIS aerosol products validation over land; *Working meeting on MERIS and AATSR Calibration and Geophysical Validation ,* 20-24 October 2003, ESA-ESRIN, Frascati, Italy,

http://envisat.esa.int/workshops/mavt_2003/MAVT-2003_502-paper_DRamon.pdf

[RD9] Leroy, M., Bruniquel-Pinel, V., Hautecoeur, O., Bréon, F. M.,Baret, F., 1998, Corrections atmosphériques des données MERIS/ENVISAT: caractérisations de la BRDF de surfaces "sombres", *European Space Agency final report*, 98 p.

[RD10]   Kaufman, Y.J., Tanré, D., 1992, Atmospherically resistant vegetation index (ARVI) for EOS MODIS. *IEEE Transactions on Geoscience and Remote Sensing*, **30**, 261-270.

[RD11]   Vermote, E.F., N., El Saleous, C.O., Justice, Y.J., Kaufman, J.L. Privette, L., Remer, J.C., Roger, and D., Tanré, 1997a. Atmospheric correction of visible to middle-infrared EOS-MODIS data over land surfaces: Background, operational algorithm and validation. *J. Geophys. Res*., **102**, 17,131-17,141.

INSTRUMENT CHARACTERISTICS

MERIS acquisition principle, in flight spectral, geometrical and radiometric calibration are described in details in **[AD4]**.

Measurement principle

MERIS is a 68.5° field-of-view push-broom imaging spectrometer that measures the solar radiation reflected by the Earth, at a ground spatial resolution of 300 m (Full resolution, or 1.2 km in Reduced resolution mode), in 15 spectral bands (see Table 1), programmable in width and position, in the visible and near infrared wavelengths. MERIS allows global coverage of the Earth in 3 days.

The Instantaneous Field Of View (iFOV) is divided into five segments, each of which is imaged by one of the corresponding five cameras. A slight overlap exists between the FOVs of adjacent optical cameras (see Fig 2). The wavelength center of each band varies along track and the amplitude of this variation reaches more than 1 nm within the FOV. An example of this "Smile" effect is given in Fig. 2 for band 1. MERIS is radiometrically calibrated onboard with a two diffuser system oriented toward the sun.

Table 1: MERIS channels

No.	Band centre (nm)	Band width (nm)	Applications
1	412.5	10	Yellow substance and detrital pigments
2	442.5	10	Chlorophyll absorption maximum
3	490	10	Chlorophyll and other pigments
4	510	10	Suspended sediment, red tides
5	560	10	Chlorophyll absorption minimum
6	620	10	Suspended sediment
7	665	10	Chlorophyll absorption & fluorescence reference
8	681.25	7.5	Chlorophyll fluorescence peak
9	708.75	10	Fluorescence reference, atmosphere corrections
10	753.75	7.5	Vegetation, cloud, O_2 absoption band reference
11	760.625	3.75	O_2 R- branch absorption band
12	778.75	15	Atmosphere corrections
13	865	20	Atmosphere corrections
14	885	10	Vegetation, water vapour reference
15	900	10	Water vapour

Figure 1: MERIS Acquisition
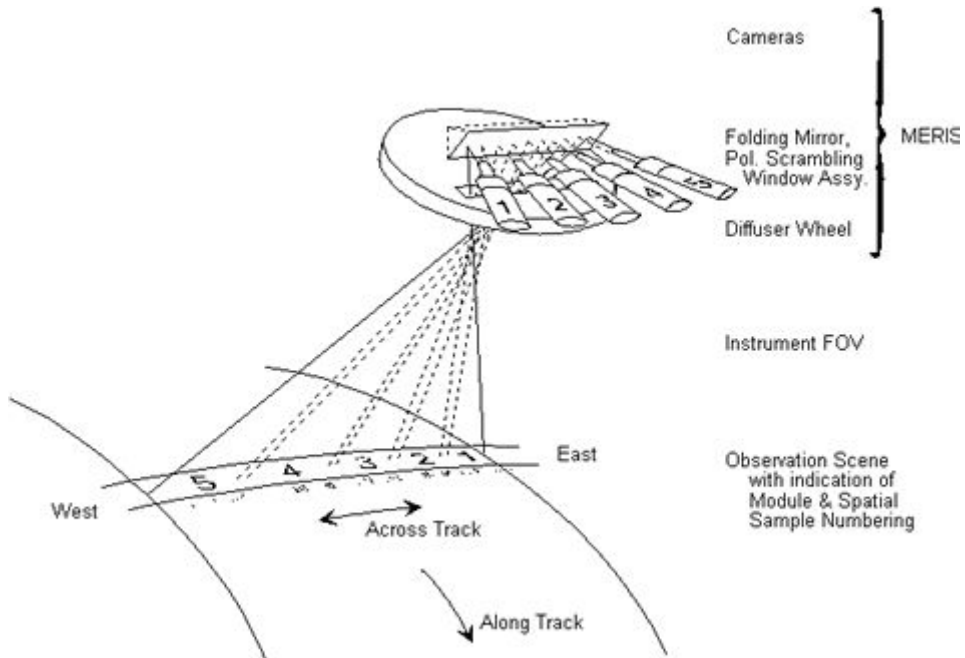
Figure 2: Spectral calibration of MERIS for channel 1 across track (below figure)
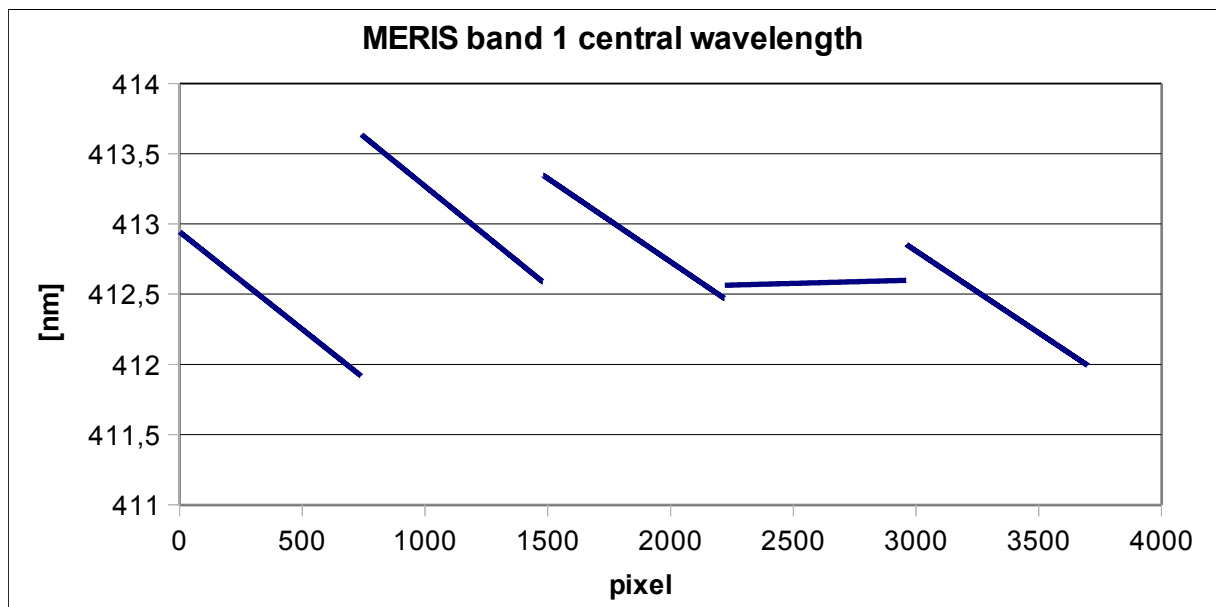
SCOPE OF THE PROBLEM

Motivation and Constraints

The aerosol product over land is designed to be simple to allow fast atmospheric corrections of MERIS L1B reflectances over land in the visible. The spectral bands of MERIS do not allow more than two aerosol parameters to be retrieved and it was decided to focus on the AOT at one wavelength and an Ångström exponent describing the spectral dependence of AOT in order to correct easily all 15 MERIS bands from aerosol contamination **[RD1]**.

A constraint is that the MERIS level 2 product is processed by a unique processor and stored in a unique file at the same spatial resolution than the level 1 data. A second constraint is to use only MERIS data.

General Approach

Aerosol remote sensing over land from space is a difficult task because of the high and variable reflectivity of Earth compared to the aerosol scattering signal in the back-scattering region. The main challenge of the algorithm is to predict from MERIS data only the surface Bidirectional Reflectance in the visible channels of MERIS.

Without the possibility to follow the MODIS approach that uses the capability to observe in the infra-red at 2100 nm for detecting dark target, the initial technique chosen relies on the detection of Dark Dense Vegetation (DDV) using a threshold on a spectral index. For MERIS the choice was to use the Atmospherically Resistant Vegetation Index (ARVI, **[RD10]**) for detecting DDV.

$$ARVI = \frac{\rho_{NIR} - \rho_{rb}}{\rho_{NIR} + \rho_{rb}} \tag{1}$$

with,

$$\rho_{rb} = \rho_r - \gamma(\rho_b - \rho_r) \tag{2}$$

where ρ_b, ρ_r and ρ_{NIR} are reflectances corrected for molecular scattering and gaseous absorption, observed respectively in the blue, red and near infra-red channels (443, 670 and 865 nm) and γ was set to 1.3, a value that reduces sensitivity of ARVI to aerosol amount **[AD6, fig.5]**.

Since the spatial coverage of DDV is low (~1% of land surfaces, on average), the aerosol retrieval has been extended to brighter surfaces, called LARS for Land Aerosol Remote Sensing targets **[RD5]**. LARS albedo at 443 and 665 nm can be predicted from the image itself using a linear relationship between the ARVI and the ground albedo **[RD2]**.

Once the surface reflectance is predicted, a simple two wavelengths aerosol optical depth retrieval is performed over each MERIS pixel and the best couple (AOT, Ångström exponent) is selected.

SCIENTIFIC BACKGROUND

We describe here the theoretical basis of the determination of the surface reflectance from MERIS data.

Surface treatment

DDV

The algorithm first used the DDV models proposed from POLDER data **[RD9]**. During January and June 1997, the clearest days have been selected using the POLDER aerosol product. This aerosol product is based on the use of the polarized radiance which is not significantly affected by a surface contribution. Because the aerosol loading was low, the classical NDVI has been initially used to identify DDV occurrences. The viewing capabilities of POLDER allow covering 12 view angles and the sun zenith angle varies along track. A canopy radiative transfer model is used to fit the data and allows extending the determination of the DDV BRDF to a large range of angles.

LARS

LARS albedo

LARS albedo at 443 and 665 nm can be predicted from the image itself using a linear relationship between the ARVI and the ground albedo. It is also true for the LARS directional reflectances **[RD5, RD2]**. The origin of such relationships deals with the direct link between the NDVI (or ARVI) and the fraction of vegetation cover. The LARS reflectance thus can be viewed as a mixture of bare soil reflectance and dark vegetation reflectance. In Fig. 3 is a typical example of such linear relationship for two location, one in Europe, the other just over Amazonian forest (almost pure DDV). As this albedo model varies with location and season, it is built on a monthly basis on a 1°x1° grid. We put a limit on the dispersion of the linear model to 0.01 r.m.s in units of reflectance. Let us notice that the LARS albedo now replaces the DDV albedo

Figure 3: Regression of spectral ground albedo for bands B1,B2,B3 and B7 vs ARVI from MERIS ALBEDOMAP data for two 1°x1° zones located in Amazonia (top) and Central Europe (bottom), for the month of June 2003. For each zone and for each linear regression (4 bands, labelled with 4 different colours), we give the wavelength, then the offset (and error), the slope (and error, after the X* sign), the ground albedo (alb$_0$) for an ARVI corresponding to DDV for that particular biome and season extracted from MERIS DDV reflectance Look Up Table and and χ, the r.m.s.e. of the fit. (below figure)
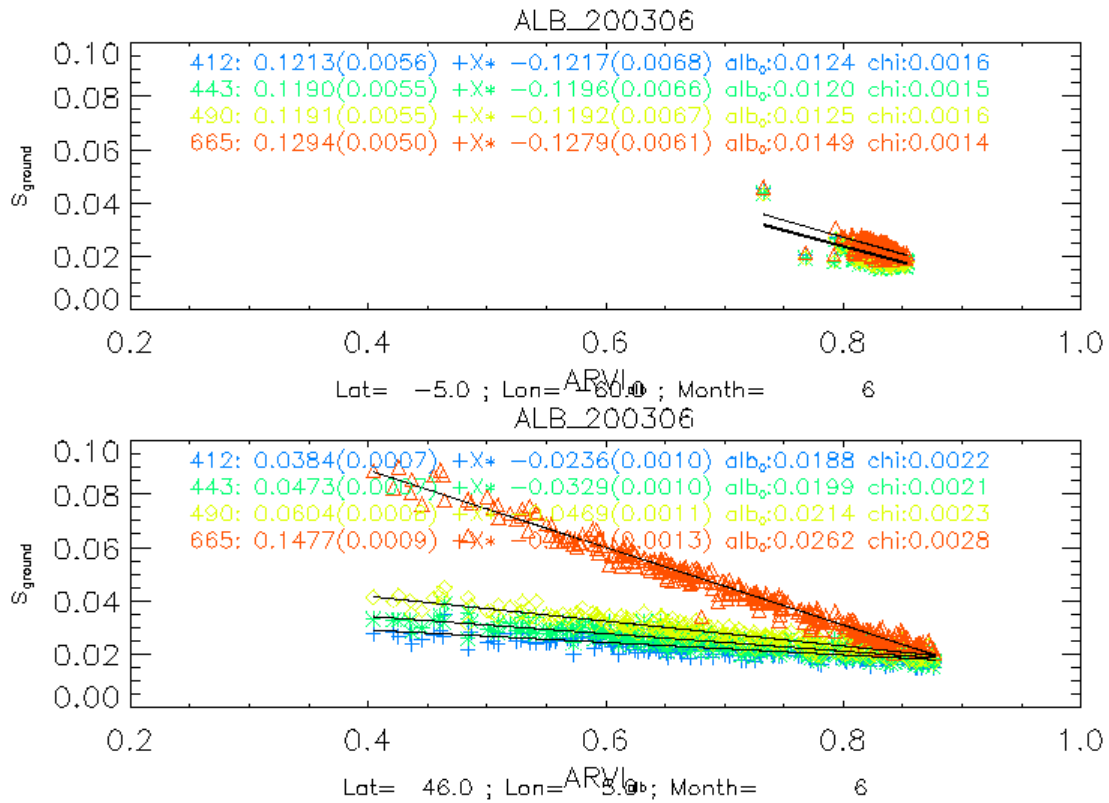
LARS BRDF

The LARS BRF is supposed to be scaled to the DDV BRF. This is a crude assumption.

$$\rho_{LARS}(\theta_s, \theta_v, \phi) = \frac{a_{LARS}(ARVI)}{a_{DDV}} \cdot \rho_{DDV}(\theta_s, \theta_v, \phi) \qquad (3)$$

the scale factor being the ratio between the LARS albedo determined from ARVI and the DDV albedo stored in LUT's

Forward radiative transfer model

The radiative transfer of the land processing was designed to run fast and easily deal with surface elevation and it is based on the following atmospheric model: the ground modelled as a DDV BRDF, an aerosol layer above, on top of that the molecular layer and finally all absorbing gases at the top (Fig 4). The accuracy of such a model was discussed in **[RD1]** and **[RD3]**.

Figure 4: Atmospheric model (below figure)

The signal follows the 6S (**[RD11]**) approach for the modelling of the couplings between the surface and the atmosphere. In this model (see Fig.5) the radiation originating from a two layers system is decomposed into 5 terms: (a) the photons from the solar beam multiply scattered in the upper layer without any other

Top Of Atmosphere ρ^{TOA}

interactions ρ^{*} Gas (H_2O, O_3, O_2)

Top Of Aerosol-Ground system ρ^{ag} Molecular scattering

Aerosols

Ground
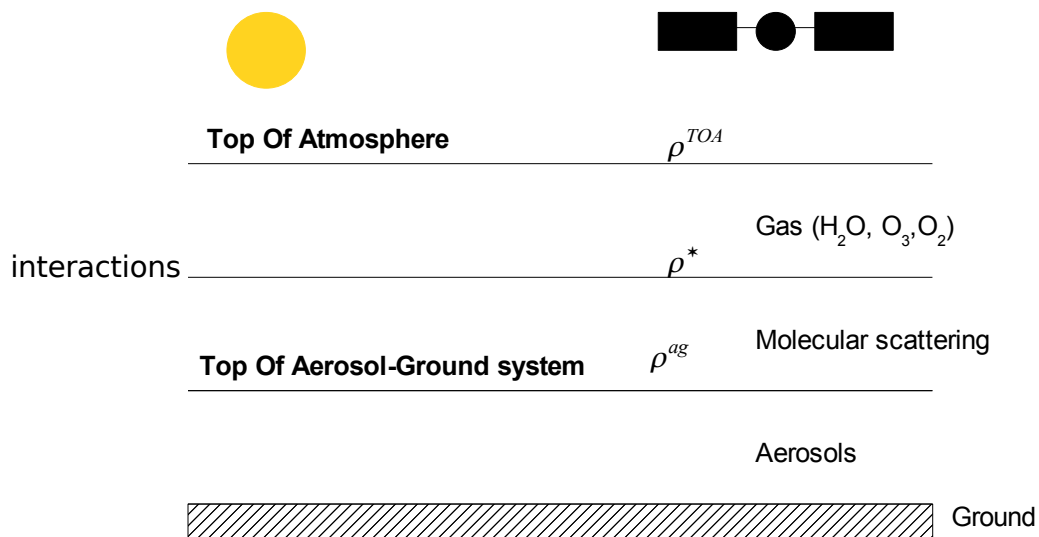
constituting the layer 1 "path radiance", (b) the photons transmitted directly to the bottom layer and directly reflected back to the sensor, (c) the photons scattered by layer 1, reflected by the bottom layer and directly transmitted to the sensor, (d) the photons directly transmitted to the bottom layer and scattered by the upper layer on their way back, (e) the photons being scattered at least twice in the upper layer.

Figure 5: The two layer 6S like radiative transfer model : (below figure)
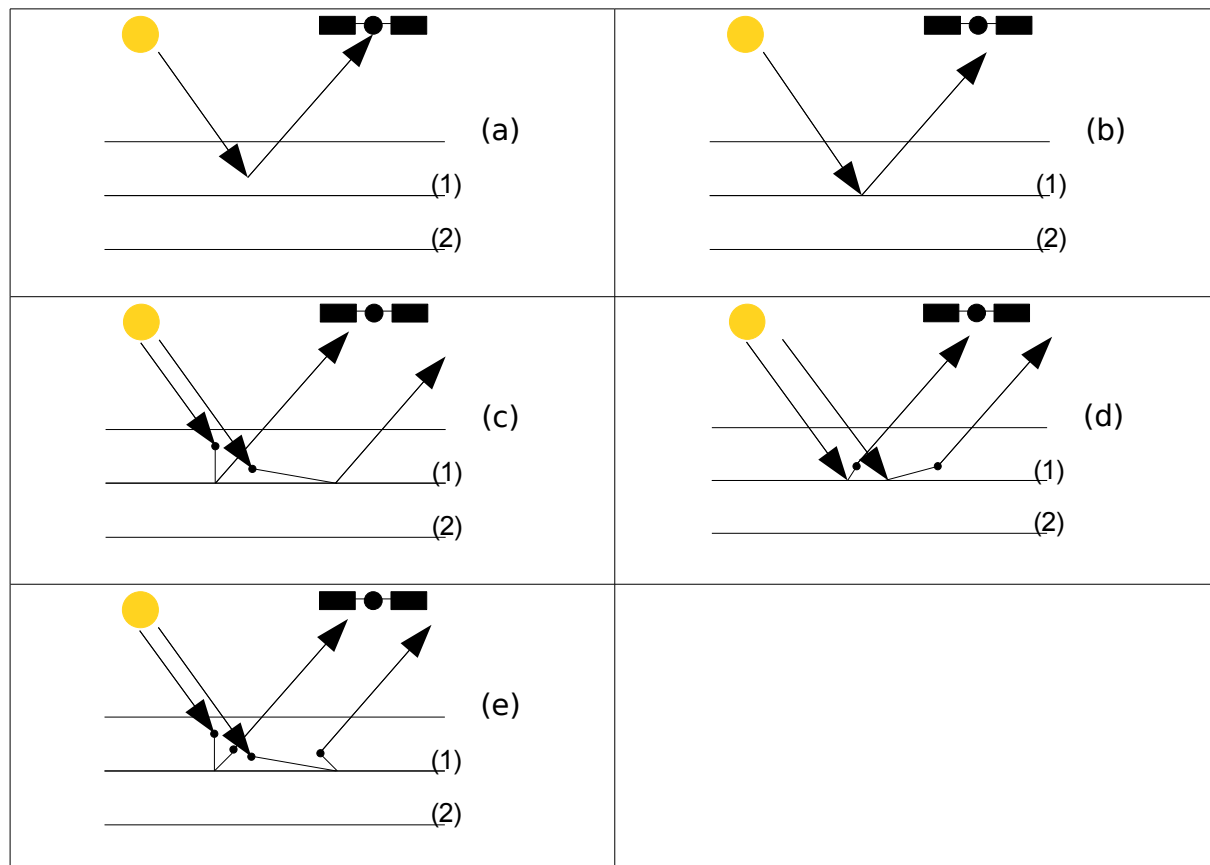
The signal at the TOA, after correction from gaseous absorption (mainly ozone) is:

$$\tilde{\rho}_g = \rho_{ag} - \rho_a = \frac{1}{1 - s_a s_g}\left(\rho_g e^{\frac{-\tau_a}{\mu_s}} e^{\frac{-\tau_a}{\mu_v}} + \overline{\rho_g}^{\downarrow a} e^{\frac{-\tau_a}{\mu_v}} t_a^{d\downarrow} + \overline{\rho_g}^{\uparrow a} e^{\frac{-\tau_a}{\mu_s}} t_a^{d\uparrow} + s_g t_a^{d\downarrow} t_a^{d\uparrow}\right)$$

(4)

$$\rho_{black} = \rho_r + \frac{1}{1 - s_a s_r}\left(\rho_a e^{\frac{-\tau_r}{\mu_s}} e^{\frac{-\tau_r}{\mu_v}} + \overline{\rho_a}^{\downarrow r} e^{\frac{-\tau_r}{\mu_v}} t_r^{d\downarrow} + \overline{\rho_a}^{\uparrow r} e^{\frac{-\tau_r}{\mu_s}} t_r^{d\uparrow} + s_a t_r^{d\downarrow} t_r^{d\uparrow}\right)$$ (5)

$$\rho^* = \rho_{black} + \frac{\tilde{\rho}_g}{1 - s_g s_r}\left(e^{\frac{-\tau_r}{\mu_s}} e^{\frac{-\tau_r}{\mu_v}} + \frac{\overline{\rho_g}^{\downarrow}}{\rho_g} e^{\frac{-\tau_r}{\mu_v}} t_r^{d\downarrow} + \frac{\overline{\rho_g}^{\uparrow}}{\rho_g} e^{\frac{-\tau_r}{\mu_s}} t_r^{d\uparrow} + \frac{s_g}{\rho_g} t_r^{d\downarrow} t_r^{d\uparrow}\right)$$ (6)

where ρ_{black} is the signal if the surface was totally black, ρ_{ag} is the signal at the top of the surface + aerosol system. These different reflectances are the sum of the atmospheric scatterers (either molecules or aerosols) path reflectance and 4 other terms describing the interaction between the surface and the scatterers

In our particular 3 layers model, we have to deal with aerosols (index a) , molecules (index r) and ground (index g) couplings. As usual It requires the computations of the aerosols (and molecular) path reflectances ρ_a and ρ_r , direct $e^{-\tau a/\mu_{s,v}}, e^{-\tau r/\mu_{s,v}}$ and diffuse transmissions t_a^d, t_r^d , spherical albedo's s_a, s_r, s_g . Additionally it requires the computations of the following coupling terms:

- $\overline{\rho}^a$: coupling terms between aerosol and molecules are in fact the weighted average over the whole hemisphere of the aerosol path reflectance by the molecular downward radiance. The approximation of an isotropic Rayleigh scattering is done for the computation and results are stored in LUT's, one for each aerosol model.

$$\overline{\rho_a}^{\downarrow r} = \overline{\rho_a}^{\uparrow r} = \overline{\rho_a}^r(\mu) = \frac{1}{2\pi}\int_0^1 \int_0^{2\pi} \rho_a(\mu', \mu, \phi')\,d\mu'\,d\phi'$$ (7)

- $\overline{\rho}_g^r$: coupling terms between molecules and the surface are in fact the weighted average over the whole hemisphere of the surface DDV BRDF by the molecular downward radiance. The approximation of an isotropic Rayleigh scattering is done for the computation and results are stored in LUT's, one for each DDV model.

$$\overline{\rho_g}^{\downarrow r} = \overline{\rho_g}^{\uparrow r} = \overline{\rho_g}^{r}(\mu) = \frac{1}{2\pi} \int_0^1 \int_0^{2\pi} \rho_g(\mu',\mu,\phi') d\mu' d\phi' \qquad (8)$$

- $\overline{\rho_g}^{a}$: coupling terms between aerosols and the surface, are in fact the weighted average over the whole hemisphere of the DDV BRDF by the aerosol downward radiance. The approximation of single scattering is done for the computation of aerosol radiance and results are stored in LUT's, one for each DDV and aerosol model doublet.

$$\overline{\rho_g}^{\downarrow a}(\mu_s,\mu_v,\phi) = \frac{\displaystyle\int_0^1 \int_0^{2\pi} p_a(\mu_s,\mu',\phi') \rho_g(\mu',\mu_v,\phi'-\phi) d\mu' d\phi'}{\displaystyle\int_0^1 \int_0^{2\pi} p_a(\mu_s,\mu',\phi') d\mu' d\phi'} \qquad (9)$$

IMPLEMENTATION

We focus here on the specific implementation aspects related to the aerosol CCI project. The reference documents for this section are [**AD9**] and [**AD8**].

<u>Note</u> : [AD9] version to be used is : issue 8, rev. 0 of 15th July 2009, that contains the updated informations describing the configuration of the level 2 processor for the 3rd MERIS reprocessing.

Cloud detection

The pixel classification is a pixel by pixel based algorithm and starts by detecting bright pixels using:

> (i) reflectance threshold at 443 nm

> (ii) thresholds on the spectral slope between the blue and the NIR of the Rayleigh corrected reflectance.

Bright pixels are considered to be cloud unless classified as snow using the MERIS Normalized Difference Snow Index MNDSI using the 865 and 890 nm channels.

The apparent surface pressure (ASP) is then estimated using the MERIS O_2 A absorption channel using a Neural Network approach with ground albedo map as auxiliary data **[AD9, section 5.1]**. A test on the difference between ASP and the estimated barometric pressure computed from ECMWF surface pressure and the terrain elevation is made to detect high clouds.

Aerosol retrieval procedure

Depending on the location and the date, one DDV model is chosen. The aerosol retrieval is performed where the LARS flag is raised, i.e. where:

> • the ARVI is greater than a minimum,

> • the LARS linear reflectance model parameters are known (see section),

> • the surface reflectance at 865 nm is greater than 0.15 to avoid shadows.

Knowing the geometry of observation and the ARVI, the surface BRDF is predicted.

Then a loop on τ_a (in the range $0 - 1.5$) at a reference wavelength of 550 nm is performed and the signal at the TOA is computed for each aerosol model in two MERIS bands: 442 nm and 670 nm. When the simulations matches the observations in the two bands, the loop is stopped and a couple of two AOT's at 412 and 670 nm AOT_{ret}^1, AOT_{ret}^2 is retrieved for each aerosol model. The selected aerosol model is the one for which the spectral dependence of the retrieved AOT's is the closest to the theoretical value of each model.

The aerosol path reflectance retrieval appears to be better at 442 nm than at 670 nm because: (i) the aerosol signature decreases with wavelength and (ii) the LARS reflectance is more accurate in the blue than in the red.

Aerosol models

From the blue and red aerosol reflectances, we can expect to derive two parameters of the aerosol model such as the aerosol optical thickness and a parameter for the size distribution. The simplest but realistic description for the size distribution is a power law:

$$n(r) = r^{\alpha-3} \tag{1}$$

where the Ångström coefficient α describes the wavelength dependency of the aerosol optical thickness τ_a :

$$\frac{\tau_a(\lambda)}{\tau_a(\acute{\lambda})} = \left(\frac{\lambda}{\acute{\lambda}}\right)^{\alpha} \tag{2}$$

Assuming a Junge power law, the phase matrix does not depend on wavelength which is of great interest in the LUTs generation.

An aerosol model is fully described by the refractive index m of the particles, the Ångström coefficient α, and the aerosol optical thickness τ_a at any wavelength.

α varies from 0 to -2.5 by step of -0.1. The aerosol scattering is assumed to be conservative (no absorption). The values of m=1.33 and 1.55 have also been computed in LUT's but are not used. By default, the refractive index is m=1.45 representing mostly continental aerosols.

Surface BRDF

DDV

There are 20 DDV models corresponding to 11 biomes in order to include seasonality.

DDV Model number	Model name	Latitude range (°)	Longitude range (°)	Month	Biome number
1	midlatitude_west_america_nov	[35, 50]	[-180, -110]	[1,2,9,10,11,12]	2
2	midlatitude_east_america_nov	[35, 50]	[-110, -30]	[1,2,11,12]	3
3	midlatitude_europe_nov	[35, 60]	[-30, 60]	[1,2,9,10,11,12]	4
4	midlatitude_asia_nov	[35, 60]	[60, 180]	[1,2,9,10,11,12]	5

				2]	
5	tropical_america_nov	[10, 35]	[-180, 40]	[1,2,9,10,11,12]	6
6	tropical_asia_nov	[10, 35]	[40, 180]	[1,2,9,10,11,12]	7
7	equatorial_america_nov	[-30, 10]	[-180, -20]	[1,2,9,10,11,12]	8
8	equatorial_africa_nov	[-30, 10]	[-20, 60]	[1,2,9,10,11,12]	9
9	equatorial_asia_nov	[-30, 10]	[60, 180]	[1,2,9,10,11,12]	10
10	boreal_america	[50, 90]	[-180, -30]	[1, …, 12]	0
11	boreal_euroasia	[60, 90]	[-40, 180]	[1, …, 12]	1
12	midlatitude_west_america_june	[35, 50]	[-180, -110]	[3,4,5,6,7,8]	2
13	midlatitude_east_america_june	[35, 50]	[-110, -30]	[3,4,5,6,7,8,9,10]	3
14	midlatitude_europe_june	[35, 60]	[-30, 60]	[3,4,5,6,7,8]	4
15	midlatitude_asia_june	[35, 60]	[60, 180]	[3,4,5,6,7,8]	5
16	tropical_america_june	[10, 35]	[-180, 40]	[3,4,5,6,7,8]	6
17	tropical_asia_june	[10, 35]	[40, 180]	[3,4,5,6,7,8]	7
18	equatorial_america_june	[-30, 10]	[-180, -20]	[3,4,5,6,7,8]	8
19	equatorial_africa_june	[-30, 10]	[-20, 60]	[3,4,5,6,7,8]	9
20	equatorial_asia_june	[-30, 10]	[60, 180]	[3,4,5,6,7,8]	10

Table 2: DDV models (above table)

Figure 6: The geographical distribution of the 11 biomes (below figure)
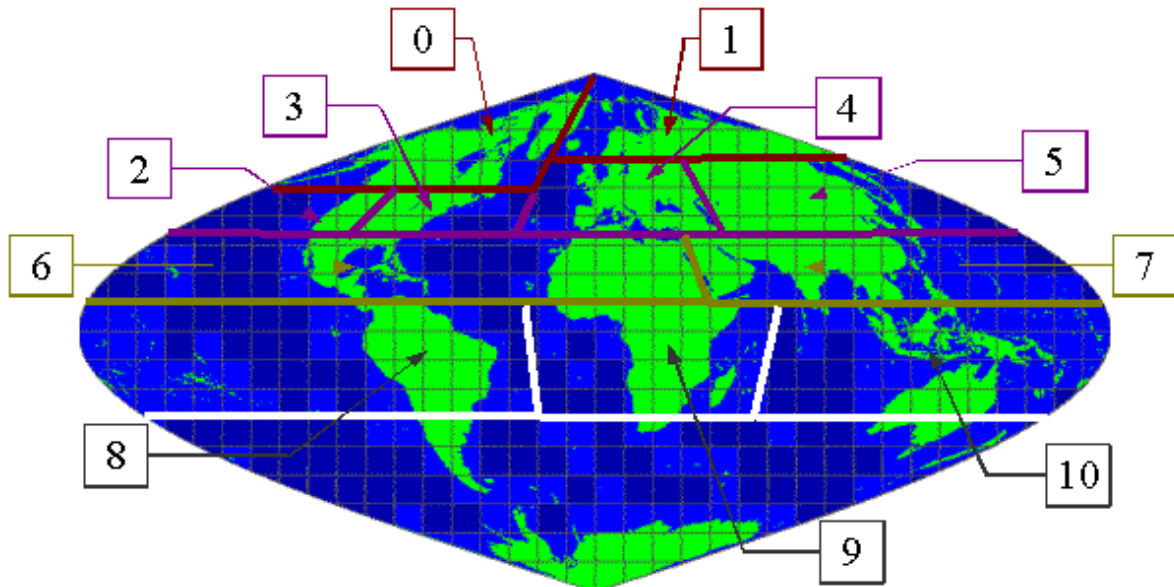
LARS albedo model

The MERIS surface albedo data from the ESA's project ALBEDOMAP are the basis for making the LARS albedo linear model (see Fig 7). We used the monthly averaged, global, white-sky (spherical, or bi-hemispherical) albedo's a_λ from the band 1 (412 nm), band 2 (443 nm), band 3 (490 nm), band 7 (670 nm) and band 13 (865 nm) generated for a rectangular grid with a box resolution of 3 arc-sec data. The year 2003 and 2005 were complete but for year 2002, we have only the period July-December and for 2006 we have January-October. The coverage of this data set is good but exclude snow covered and permanently cloud covered areas.

For each month, in a 1°x1° super-box (with 20x20=400 points), a linear regression of the Atmospherically Resistant Vegetation Index (ARVI) versus the spectral white sky albedo's a_λ for bands B1,B2,B3 and B7 is performed. ARVI is computed using equations (1) and (2) with white sky albedo's a_λ instead of directional reflectance ρ_λ

The regression parameters for each month are then averaged over available years in order to reduce the noise and fill gaps. Finally the Look Up table consists of the following quantities:

1. C(b) for b=B1,B2,B3,B7 that is a derived parameter giving the ratio between the LARS spherical albedo when ARVI= $ARVI_{DDV}$ and the DDV spherical albedo. $ARVI_{DDV}$ is calculated from DDV spectral spherical albedo, themselves being computed from DDV spectral directional reflectance stored in MERIS DDV LUT.

2. S(b) for b=B1,B2,B3,B7, the regression slopes.

3. $DARVI_{MIN}$, the threshold for the quantity (ARVI - $ARVI_{DDV}$), above which the LARS reflectance model is considered robust enough to allow an aerosol retrieval.

4. $DARVI_{MAX}$, the threshold for the quantity ($ARVI - ARVI_{DDV}$), above which the LARS reflectance does not vary any more with ARVI and is taken constant

An example of the LARS albedo estimated from this linear model is given in Fig 8 where the rms error attached to the fit is also plotted. This gives an idea about the spatial cover of the LARS model as well as its typical accuracy which depends strongly upon location and season

Figure 7: The LARS albedo linear model (below figure)
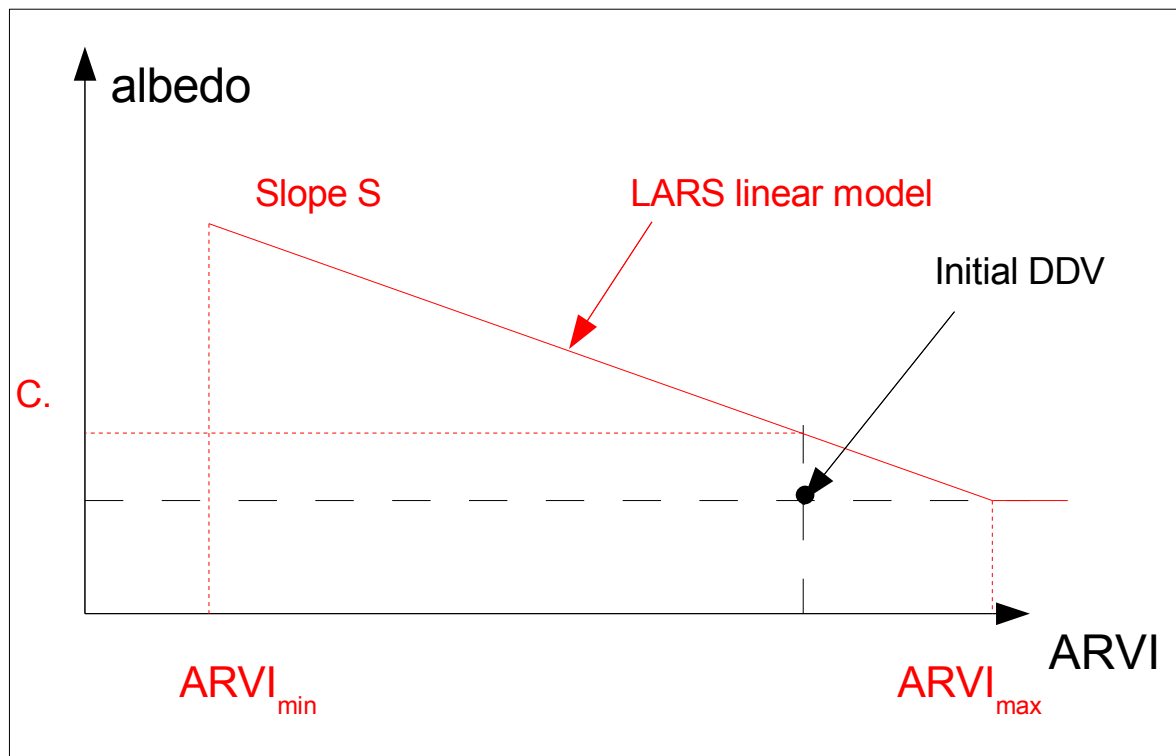
Figure 8: LARS albedo at 665 nm for an ARVI of 0.6 for the month of July (top, with a scale between 0 and 0.01) and r.m.s. of the linear model (bottom, with a scale between 0 and 0.01)
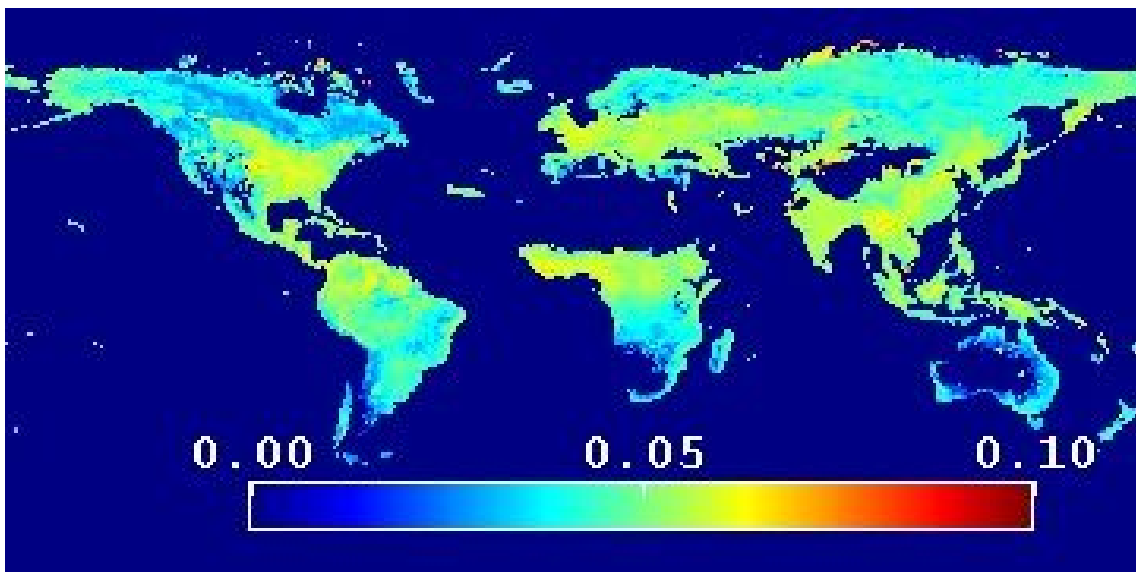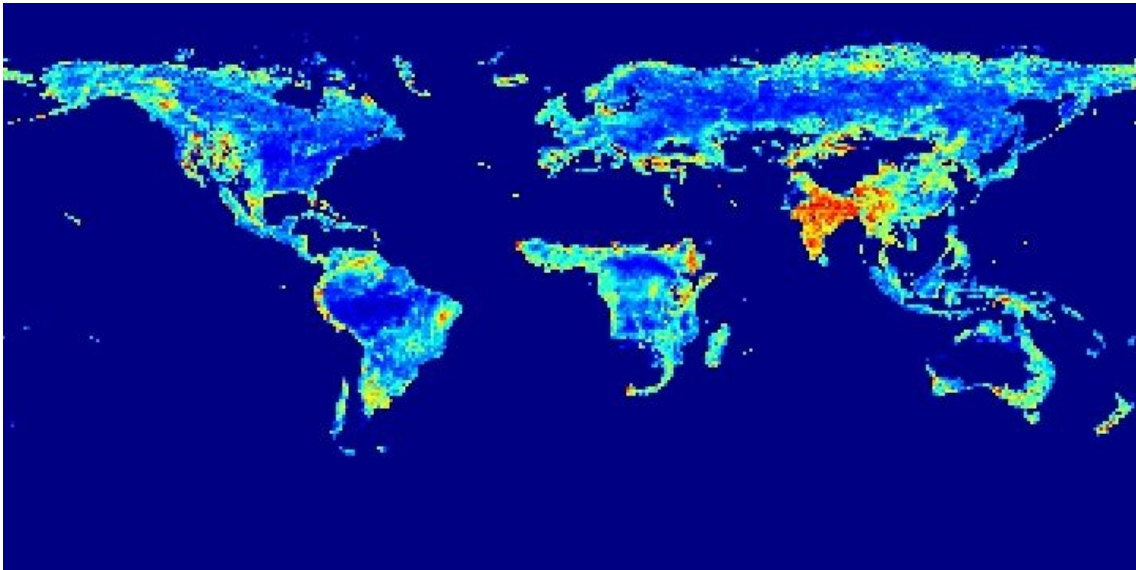
INPUT DATA REQUIREMENTS

The MERIS level 1B and level 2 auxiliary data products are described in details in **[AD4]** and **[AD8], [AD13]**

The MERIS L1B data includes all necessary ancillary data to run the algorithm:

- Digital elevation model (cloud mask, Rayleigh optical thickness)

- Atmospheric pressure at the sea-level (cloud mask, Rayleigh optical thickness) and wind speed (glint)

- Ozone column amount (absorption correction)

The MERIS accurate spectral model is also necessary to perform the "smile" effect correction of L1B radiances as well as the computation of apparent surface pressure with the O_2 A band.

All Look Up Tables are stored in different files (level 2 auxiliary data). The important tables impacted in the aerosol cci project are :

- Aerosols scattering functions (climatology of refractive index, phase function, transmissions, spherical albedo, multiple scattering ratio, aerosol-Rayleigh coupling functions...)

- DDV (BRDF, DDV aerosol coupling functions, DDV Rayleigh coupling functions, ARVI thresholds)

- LARS (ARVI min and max, slope and offset of the LARS albedo linear model)

OUTPUT

The MERIS level 2 product is described in **[AD11]** and **[AD9]**

The aerosol product is a small part of the level 2 product file and is at the same resolution that the level 1 product (i.e. at 1.2 km in Reduced Resolution mode)

It consists of :

- Over land

    - the retrieved AOT in the product is given at 443 nm. this AOT is derived from the top of Rayleigh reflectance using the aerosol model with $\alpha=-1$.

    - the Ångström exponent α in the product corresponds to the aerosol model selected as the result of the best fit at 443 nm and 670 nm.

- Over ocean

    - the AOT retrieved by the ocean branch algorithm is given at 865 nm

    - the Ångström exponent α in the product corresponds to the aerosol model selected as the result of the best fit at 865 nm and 778 nm.

- A quality flag named "PCD_19", when it is raised (=1), the quality is bad due for example to an out of bound value for the AOT or Ångström exponent.

ERROR BUDGET ESTIMATES

Aerosol model

The error associated with the aerosol model is addressed in **[RD8]** and **[RD7]**.

The error due to the choice of the Junge power law size distribution is on average not far from 15% in estimating the aerosol path reflectance, except for large dust episodes.

The MERIS measurement is insensitive to absorption and therefore should lead to larger under estimation of the AOT in case of smoke events. The kind of error associated with the aerosol model choice is mainly a regional/seasonal bias.

Surface

Surface albedo

As shown in Fig 8, the LARS albedo estimation accuracy is limited to 0.01 by construction but depends on location and season. The accuracy decreases also with the brightness of the target and thus the best case is a vegetated area at 443 nm.

A typical accuracy at 443 nm is close to 0.003 in reflectance unit, translating into an AOT error of 0.03

The kind of error associated with the surface albedo is mainly random noise, with a strong regional/seasonal amplitude variation. The estimation of this error could be made from the rms of the linear fit during the build up of the LARS albedo LUT's

Surface BRDF

We have no estimation of the error associated with the wrong estimation of the LARS BRDF. It is clear however that it increases with decreasing ARVI (departure from pure DDV) or increasing brightness.

Cloud Contamination

This is the major issue with the AOT accuracy and can be estimated only after a vast statistical comparison with AERONET data. A good way of dealing with this error source is to share a common cloud mask between different algorithms/sensors. A good quality indicator for the aerosol retrieval is the distance of the inverted pixel to the closest identified cloud

PRACTICAL CONSIDERATIONS FOR IMPLEMENTATION

Implementation

The implementation is done through the ENVISAT IPF routinely. See **[AD12]** for IPF configuration monitoring

Validation

The recommendations we made for further use of the product by the users:

Average the product over 10 km spatial resolution (like level 2 of MODIS) and filter out macro pixels with large local variance of AOT and/or high difference between apparent surface pressure and barometric pressure. This can be done with the BEAM software.

Good performances can be achieved with current macro-pixels AOT at 443 nm over land, when compared to AERONET and MODIS **[RD 8][RD 4]**.

Ångström exponent, more sensitive to instrument and algorithm noise is not validated, should be retrieved in the future on a macro pixel basis only and is not validated at the moment.

Figure 9: Validation of the Aerosol Optical Thickness at 443 nm retrieved by MERIS versus AOT measured by 39 AERONET stations during the period 2002-2007. Macro pixels (12x12 km) with local standard deviation of the AOT greater than 0.1 or difference between apparent surface pressure and barometric pressure greater than 40 hPa are discarded. (below figure)

total
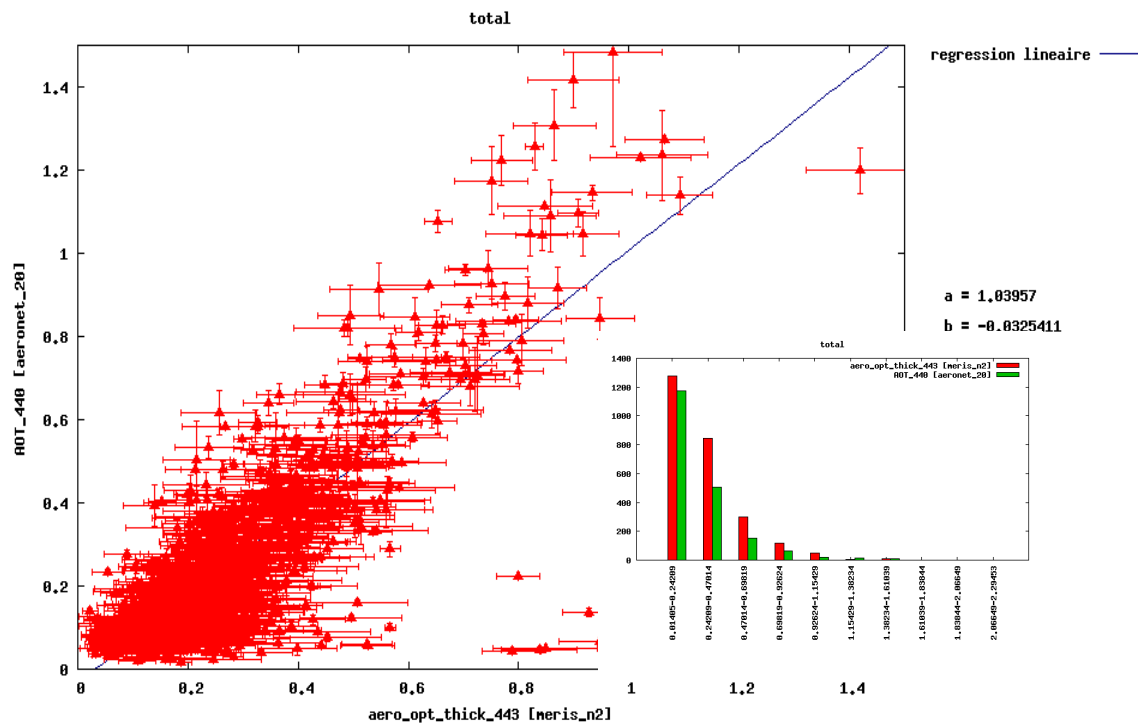
CONCLUSIONS

BRDF

The algorithm over land is now quite complex. Incoherence between the "old DDV BRDF models" and the new LARS BRDF should be fixed. One possible way to do so is to consider LARS BRDF to be a weighted average between bare soil BRDF and DDV BRDF, the weight being determined from the measured ARVI. Another one is to directly import BRDF climatology as auxiliary data.

The computation speed that was the main argument in 1997 for decoupling aerosols and molecules is not necessary anymore in 2011. One could compute all atmospheric terms and couplings with the ground using a realistic aerosol and molecules mixture, depending on aerosol model, aerosol load, and surface elevation (or barometric pressure).

Auxiliary data for computing LARS albedo linear model LUT's should be the least possible contaminated by clouds.

Cloud Contamination

Cloud contamination is still the biggest issue and the product should benefit from the aerosol-cci project to clarify how to reject more efficiently clouds.

Spatial resolution

The spatial resolution of 10 km for the aerosol product is mandatory, and there is no reason to keep it at the level 1 resolution. The main reason is to allow additional filtering (mainly cloud contamination) and to enhance the SNR ratio for the aerosol model determination.

End of the document